Influence of the average roughness Rms on the precision of the Young's modulus and hardness determination using nanoindentation technique with and Berkovich indenter

Mounir Qasmi, Patrick Delobelle

Influence of the average roughness Rms on the precision of the Young's modulus and hardness determination using nanoindentation technique with a Berkovich indenter

M. Qasmi, P. Delobelle*

Institut FEMTO-ST, Laboratoire de Mécanique Appliquée R. Chaléat, UMR 6174 CNRS, Université de Franche-Comté, 24, chemin de l'Epitaphe, 25000 Besançon, France

Using a compilation of experimental results obtained on different materials, the influence of the average roughness R_{ms} on the precision σ_E (standard deviation) of the Young's modulus (E_{mean}) determination using the Berkovich nanoindentation technique is studied for different depth penetration h. A power law dependence such as $\sigma_E / E_{mean} = \beta(R_{ms} / h)^n$ with $n = 0.67$, seems to be adapted. The value of this exponent, which is slightly function of the roughness fractal dimension, is in accordance with the works of Bobji et al. [M.S. Bobji, K. Shivakumar, H Alehossein, V. Venkateshwarlu, S.K. Biswas, Int. J. Rock Mech. and Min. Sci. 36 (1999) 399]. Nevertheless, the value of β is higher than the one given by those authors for millimetric scale of the relief and for a spherical indenter shape. For the hardness H, the following relation can be written, $\sigma_H / H_{mean} = \delta\sigma_E / E_{mean}$ with $1.2 \leq \delta \leq 2$ according to the material, the presence and the nature of the substrate.

Keywords: Nanoindentation; Young's modulus; Hardness; Roughness; Scatter

1. Introduction

During the experimental determination of the Young's modulus, using the nanoindentation technique [1–4] on bulk materials and thin films, the precision of the results is strongly depending on the surface quality of materials which can be characterised by its fractal dimension D and its roughness R_{ms} [5–8]. According to the elaborating ways of material in the case of thin films (electroplated, sputtering, PECVD, LPCVD,...) and the conditions of machining or polishing of bulk materials, these two parameters can evolve in great range. Actually only few studies are done in this way, especially in the case of nanoindentation using a Berkovich tip, but we can still quote works of Bobji et al. [6–8] which were carried out at macroscopic scale ($R_{ms} \approx 1$ mm), for different shape of asperities and using a spherical indenter. Those authors report the following relationship for the hardness H_{mean} of several materials:

$$\frac{\sigma_H}{H_{mean}} = \beta\left(\frac{R_{ms}}{h}\right)^n \quad (1)$$

where σ_H is the standard deviation for a number of measurement higher than 25 and h is the indentation depth [6,7]. The aim of the present paper is to study, on few thin films and on bulk materials with roughness at nanometric scale ($2 < R_{ms} < 200$ nm), the expressions $\frac{\sigma_E}{E_{mean}}$ and $\frac{\sigma_H}{H_{mean}}$ and compare them with results brought back by Bobji et al. [6,7].

Having carried out many tests of nanoindentation on various materials whose surface qualities, primarily characterised by their roughness R_{ms} (which are very different), we suggest to carry out an analysis of the results to evaluate the influence of this roughness, according to the depth penetration, on the precision of the determination of the Young's modulus E_{mean} and the hardness H_{mean}.

* Corresponding author. Tel.: +33 381 66 60 13; fax: +33 381 66 67 00.
E-mail address: patrick.delobelle@univ-fcomte.fr (P. Delobelle).

2. Experimental techniques and studied materials

The nanoindentation tests of the Berkovich type were carried out on a nanoindenter II^S, (Nanoinstrument) using the continuous stiffness method (CSM) that allows to obtain the values of the Young's modulus E and hardness H according to the indentation depth h. Thus, during the indentation, the indenter vibrates at a frequency of 45 Hz with an amplitude order of the nanometer, what allowed to measure, moreover the load P and the depth indentation h, the contact stiffness S during the indentation sequence.

E and H are calculated according to the Oliver and Pharr method [3] and are expressed as follows:

$$\left(\frac{dP}{dh}\right)_{unload} = S = \frac{2\eta}{\sqrt{\pi}} E_r \sqrt{A} \text{ with } \frac{1}{E_r} = \frac{1-\nu^2}{E} + \frac{1-\nu_i^2}{E_i}$$
$$H = \frac{P}{A} \text{ with } A(h_c) = 24.5h_c^2 + \sum_{n=1}^{4} (a_n h_c^{1/n}) \text{ and } h_c = h - \varepsilon \frac{P}{S} \quad (2)$$

In these expressions $\eta = 1.034$ for a Berkovich indenter, $\varepsilon = 0.72$ for a conical indenter and h is the measured total displacement. A is the projected remanent surface, E and ν the elastic modulus and the Poisson's ratio of material and E_i, ν_i, the same parameters for the indenter ($E_i = 1141$ GPa, $\nu_i = 0.07$). $S = (dP/dh)_{unload}$ is the unloading stiffness at the depth h.

In Table 1 are mentioned the studied materials (Mat.), the technical elaboration (Elabor.), the substrate for thin films (Subst.) and some informations about the grains size diameter (ϕ) and the crystallite orientations <hkl> (Struct. inf.) as well as films thickness (e_f), average roughness (R_{ms}), studied range (h), number of measurements on each sample ($\sum$) and at last references of published work (Ref.)

On each sample, 25 to 45 indents were carried out on two or three different zones ($\approx 15 \times 2$ or $\approx 15 \times 3$ indents approximately) and the indents are sensibly spaced to 50 μm. Then, the average values E_{mean} and H_{mean} are calculated as well as the standard deviations which are associated to σ_E and σ_H. It will be noted that according to Bobji et al. [7] the value of the standard deviations becomes independent on the indentation number from about twenty five measurements, which is carried out here (Table 1, $\sum$).

The roughness R_{ms} and the morphology of surfaces were studied by an atomic force microscope (AFM) in contact mode. An area of $4 \times 4\,\mu m^2$ or $10 \times 10\,\mu m^2$ was scanned at different places (3 or 4 places) in the surface in order to make sure that the images taken in AFM are representative of the film surface. For the roughest materials ($R_{ms} > 50$ nm), measurements were carried out using a confocal microscope on a surface of $50 \times 50\,\mu m^2$, and also on two or three different places. It is interesting to notice that the analysed surface should be at least twice bigger than the imprint, in our case it is $50h^2$. Three ceramics PZT, PMNT, AlN and several metals, Cr, W, Ni were studied.

(i) Ceramics PZT and PMNT are obtained by RF magnetron sputtering from cold pressed power target and give thin

Table 1
Studied materials

Mat.	Substr.	Elabor.	Struct. inf.	e_f (nm)	R_{ms} (nm)	h (nm)	$\sum$	Ref.
PZT	$Pt/TiO_2/SiO_2$	rf magn. sput	$\phi = 4\,\mu m$, <110>	980	5.5±0.5	25–300	28	[9,10]
PZT	$Pt/TiO_2/SiO_2$	rf magn. sput	$\phi = 1\,\mu m$, <111>	805	5.5±0.5	25–300	26	[9,10]
PMNT	$Pt/TiO_2/SiO_2$	rf magn. sput	–	620	35.5±5	25–300	28	–
W	SiO_2/Si	dc magn. sput	Dom. size 50 nm, <110>	1000	6.0±0.5	50–700	26	[12,13]
W	SiO_2/Si	dc magn. sput	Dom. size 50 nm, <110>	1000	5.2±0.5	50–700	27	[12,13]
W	SiO_2/Si	dc magn. sput	Dom. size 50 nm, <110>	1000	7.5±0.5	50–700	45	[12,13]
W	SiO_2/Si	dc magn. sput	Dom. size 50 nm, <random>	1000	5.4±0.5	50–700	29	[12,13]
AlN	Glass	Reactive sput	$\phi = 0.3\,\mu m$ <001>	1180	2.0±0.5	10–200	23	–
Cr	Si<100>	dc magn. sput	$m = 1$, $\alpha = 0°$	1027	6.8±1.4	50–700	25	[14,15]
Cr	Si<100>	dc magn. sput	$m = 1$, $\alpha = 10°$	971	8.7±1.2	50–700	27	[14,15]
Cr	Si<100>	dc magn. sput	$m = 1$, $\alpha = 20°$	874	6.9±0.2	50–700	23	[14,15]
Cr	Si<100>	dc magn. sput	$m = 1$, $\alpha = 30°$	986	9.3±0.9	50–700	28	[14,15]
Cr	Si<100>	dc magn. sput	$m = 6$, $\alpha = 10°$	1228	4.1±0.3	50–700	24	[14,15]
Cr	Si<100>	dc magn. sput	$m = 6$, $\alpha = 20°$	1143	5.5±0.5	50–700	26	[14,15]
Cr	Si<100>	dc magn. sput	$m = 6$, $\alpha = 30°$	1198	4.2±0.6	50–700	25	[14,15]
Cr	Si<100>	dc magn. sput	$m = 6$, $\alpha = 20°$	971	4.4±0.3	50–700	28	[14,15]
Ni	Bulk	Cast	$\phi = 150\,\mu m$, <111>	–	14.9±5.2	25–125/25–900	41	[16,17]
Ni	Bulk	Cast	$\phi = 150\,\mu m$, <110>	–	14.9±5.2	25–125/25–900	47	[16,17]
Ni	Bulk	Cast	$\phi = 150\,\mu m$, <100>	–	14.9±5.2	25–125/25–900	33	[16,17]
Ni	Ti/Cu	Electr. plated $J = 0.39$ A dcm^{-2}	$\phi = 0.38\,\mu m$, random	$2.1.10^5$	90±25	250–1650	37	[16,17]
Ni	Cu	$J = 0.13$ A dcm^{-2}	$\phi = 0.22\,\mu m$, random	$4.0\ 10^5$	49±15	600–900	26	[16,17]
Ni	Cu	$J = 0.62$A dcm^{-2}	$\phi = 0.61\,\mu m$, random	$4.0\ 10^5$	130±31	700–1150	25	[16,17]
Ni	Cu	$J = 3.01$A dcm^{-2}	$\phi = 0.86\,\mu m$, random	$4.0\ 10^5$	195±35	850–1400	25	[16,17]
Ni	Ti/Cu	$J = 2.5$ A dcm^{-2}	$\phi = 1.03\,\mu m$, random	$2.0\ 10^5$	159±32	250–1800	37	[16,17]

Mat.: studied materials; Elabor.: technical elaboration; Subst.: substrate for thin films; Struct. inf.: the crystallite orientations <hkl>; ϕ: some information about the grains size diameter; e_f: films thickness; R_{ms}: the average roughness; h: the studied area; $\sum$: number of measurements on each sample; Ref.: references of published work.

films of 0.6 to 1 μm thick [9,10]. The substrates used are platinized silicon, Pt/Ti/SiO_2/Si. Ceramics PZT present a roughness R_{ms} of 5 to 6 nm, whatever the grains diameter ($0.2<\phi<4$ μm) and an average modulus for $h/e_f \approx 2.5\%$ of 125 GPa for $\phi=4$ μm and of 138 GPa for $\phi=1$ μm (Fig. 1). On the other hand, the roughness of PMNT ceramics raises (we observe several disordered crystallites), typically it varies from 35 to 40 nm for a modulus of 140 GPa [9]. The high values of E_{mean} can be explained by the ferroelectric reorientation domain under indentation stresses [10].

(ii) AIN is obtained by reactive sputtering and the used substrate is glass. This ceramic presents a small roughness of 2 nm and the crystallites are well oriented along <001>. For $h/e_f \approx 0.8\%$ ($h \approx 10$ nm), the modulus value is 320 GPa (Fig. 1), which correspond to the value that can be computed for this orientation using the C_{ij} compliances of this material [11].

(iii) Tungsten is also obtained by DC magnetron sputtering and results in a thin film of approximately 1 μm thick deposited on a Si<100> substrate [12]. According to the deposition conditions and especially the Xenon pressure in the reactor, the mechanical properties as well as roughness evolve. Thus, the average Young's modulus E_{mean} and roughness R_{ms} decrease with the Xenon pressure; $385<E_{mean}<435$ GPa for $h/e_f \approx 5\%$ and $5.2<R_{ms}<7.5$ nm when $0.4<P_{Xe}<1$ Pa [13]. For a bulk material, the modulus value is 410 GPa, the measured values on thin films can be explained by the presence of residual stresses [13].

(iv) Cr is obtained by DC magnetron sputtering with glancing technical angle deposition and appears like a thin film of approximately 1 μm thick composed of various layers whose thickness and inclination are variable. The substrate is Si<100> [14]. According to the deposition conditions, number of layers m and angle of inclination α, the average Young's modulus for $h/e_f \approx 10\%$ varies from 140 to 230 GPa for $\alpha=17°5$ and $1<m<20$, from 80 to 165 GPa for $\alpha=25°5$ and $1<m<20$. The roughness varies respectively from 4.4 to 6.9 nm and from 6.2 to 9.4 nm under these same conditions [14]. For higher slope, the porosity can be very important [15] and in this study we only consider thin films that present porosity smaller than 10%. In this case, considering this porosity, we find roughly the bulk Cr modulus value, which is 265 GPa.

(v) Two types of Ni were studied. Firstly, bulk Ni with large grains ($\phi \approx 150$ μm), hardened or recrystallized states, and whose final surface quality is obtained by electrolytic polishing leading to a mean roughness about 15 nm, slightly function of the grains orientation. An EBSD study allows to specify the orientation of the grains, which makes it possible to carry out nanoindentation tests on grains whose orientation is known, especially <100>, <110> and <111>. The modulus values depend on this orientation [16] and are calculated between 214 (<100>) and 235 GPa (<111>). The second type of Ni is obtained by electroplating and results in thick films of approximately 200 or 400 μm thick deposited on Ti or Cu substrates. According to the electroplating conditions and especially to the current density J, $0.13<J<4.1$ A dm^{-2}, the grains size as well as the mechanical properties evolve in a considerable way and an Hall–Petch relationship on hardness is reported [16,17]. A linear relation between the grain diameter and roughness is clearly highlighted [17,18]. An R_{ms} study with the AFM in four different places of the samples, on a surface of $10\times10\,\mu m^2$, leads to $R_{ms}=90\pm25$ mm for $J=0.39$ A dm^{-2} and $R_{ms}=159\pm32$ nm for $J=2.5$ A dm^{-2}. For the other samples, values of R_{ms} were determined using a confocal microscope on an area of $50\times50\,\mu m^2$ and on three different places. These values are raised enough and characteristic of the surface quality of materials obtained by electroplating. The

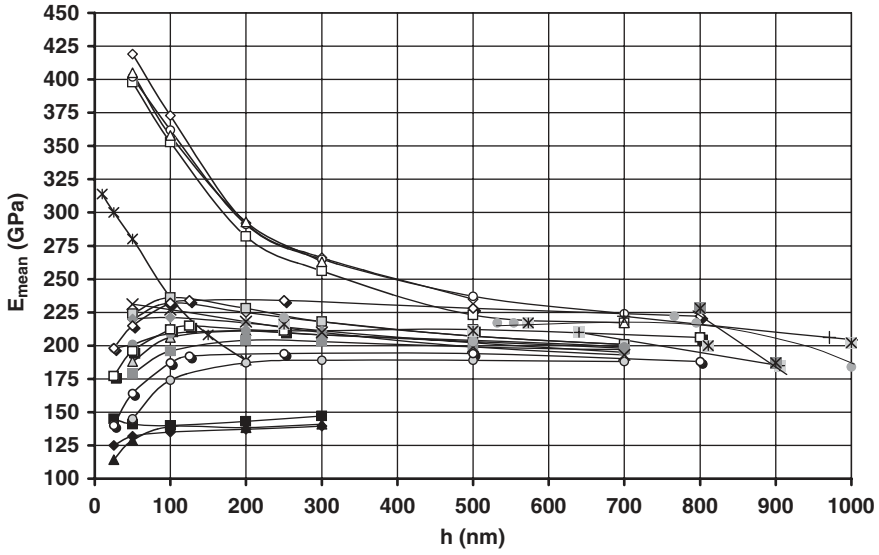

Fig. 1. Evolution of E_{mean} versus h for different materials.

measured moduli decrease when the current density J is increasing and we report $178 < E_{mean} < 230$ GPa for $0.13 < J < 4.1$ A dm^{-2} [17,19].

In conclusion, this study cover modulus values included between 120 and 425 GPa (Fig. 1).

Note that the average values of the Young's moduli previously reported correspond, in the case of thin films, to those given for very low depths penetration ($h/e_f \leq 5\%$) and approximately represent the intrinsic values of considered material. The substrate affects very quickly, as soon as few percent of h/e_f, the Young's modulus determination (Fig. 1) [20–22].

In the following study, the considered values of E_{mean} are those measured for a fixed indentation depth (h=25, 50, 100, 200, 300, 500, 700, 1000 and 1500 nm) which take into account the nature, the thickness and the mechanical properties of the film as well as elastic characteristic of the substrate.

3. Results and analysis

The presented analysis assumes that the precision of the obtained results depends essentially upon the surface roughness and the indentation depth and that all other factors have only minor influences. Indeed, for the lower penetration depths, the area function introduced in Eq. (2) ($\sum_n a_n h_c^n$) is artificial and requires a functional relationship on a physical body (the indenter) which do not have any real justification. Thus the area function is likely to have a far greater amount of experimental variations associated with it at the lower penetration depths compared with larger depths; these variations are likely to lead to a loss of precision in the results obtained on the different materials. Moreover, at very low loads, variations in the area function deduced from h_c, not only depends on the surface roughness but also on the limitations of the instrument, e.g., electronic noise during the surface detection procedure, digitization errors,…. In the present study, the smallest considered indentation depth is h_c=25 nm and the two previous effects are supposed to have only minor repercussions on the experimental results. This conclusion seems 'a posteriori' verified in Fig. 5, the scatter in the data at $R_{ms}/h \approx 20\%$ is not really greater than those at $R_{ms}/h \approx 1\%$.

Figs. 1–3 present respectively for all studied materials and for $25 < h < 1000$ nm the variation of E_{mean}, σ_E the standard deviation and the ratio σ_E/E_{mean} (relative standard deviation). We easily observed that σ_E and σ_E/E_{mean} are decreasing functions of h. On the other hand, for the same indentation depth, only σ_E/E_{mean} seems to be an increasing monotonic function of R_{ms} and not of σ_E. This observation is highlighted on Figs. 2 and 3 for h=25 or 50 nm.

Fig. 4(a, b) present two examples, for small (h=50 nm) and high (h=700 nm) depths penetration, of the variation of σ_E/E_{mean} according to the roughness for various tested materials, except electroplated Ni on Fig. 4a where the modulus values were measured starting from h=250 nm. σ_E/E_{mean} is obviously an increasing function of R_{ms} and the whole points, in spite of the scattering aspect, seems to gather around a main curve. Continuity exists between data that correspond to thin films and to bulk materials. For each studied indentation depth, looking for a power law such as $\sigma_E/E_{mean} = a(R_{ms})^{n_1}$, n_1 is obtained equal to 0.71 ± 0.05 and writing the variation of 'a' versus h such as $a = a_0 h^{-n_2}$, we obtain $n_2 = 0.66 \pm 0.02$. Exponent n_1 and n_2 being close, $n_1 \approx n_2 = n$, it seems possible to write the following relation:

$$\frac{\sigma_E}{E_{mean}} = \beta \left(\frac{R_{ms}}{h} \right)^n \text{ with } 0.66 < n < 0.71 \quad (3)$$

This relation can be verified on Fig. 5 where all experimental points are aligned in Ln–Ln representation, whatever the

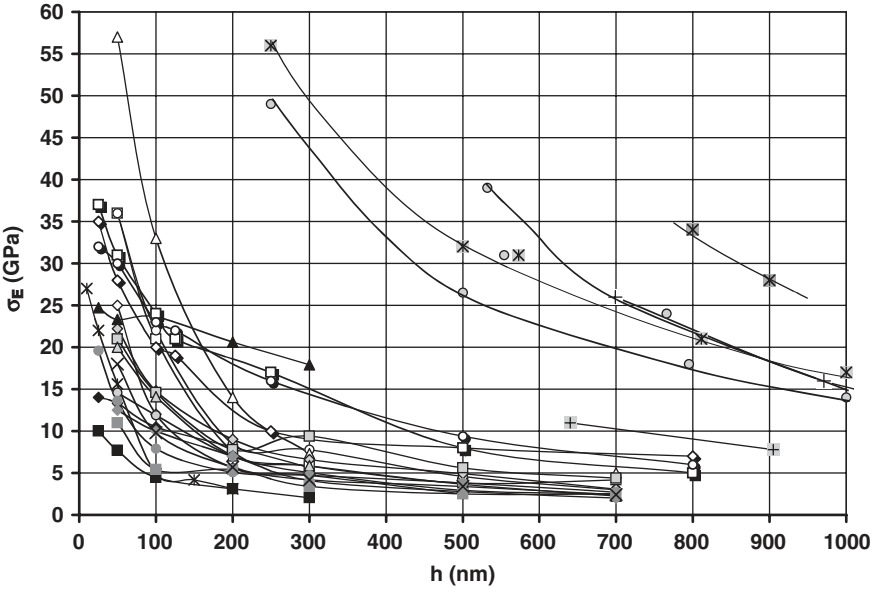

Fig. 2. Evolution of the standard deviation σ_E versus h for different materials.

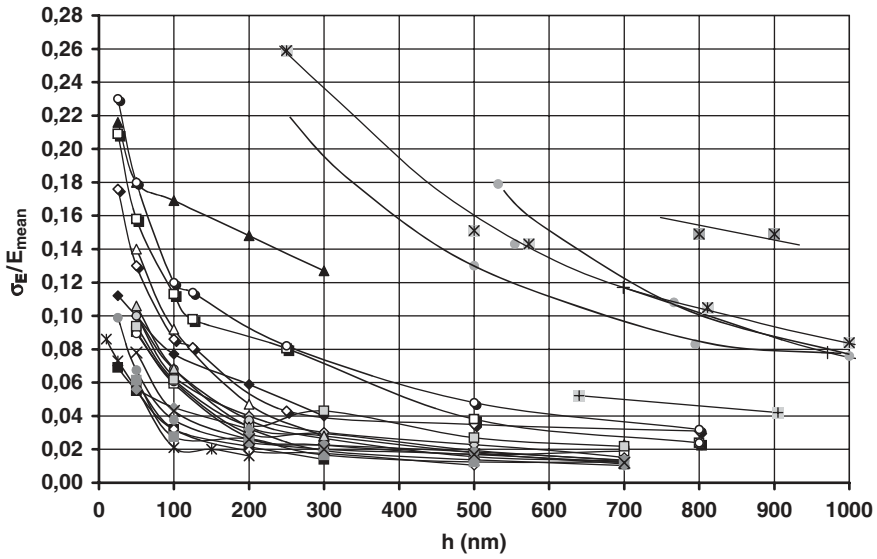

Fig. 3. Variation of the ratio σ_E/E_{mean} versus h for the different materials.

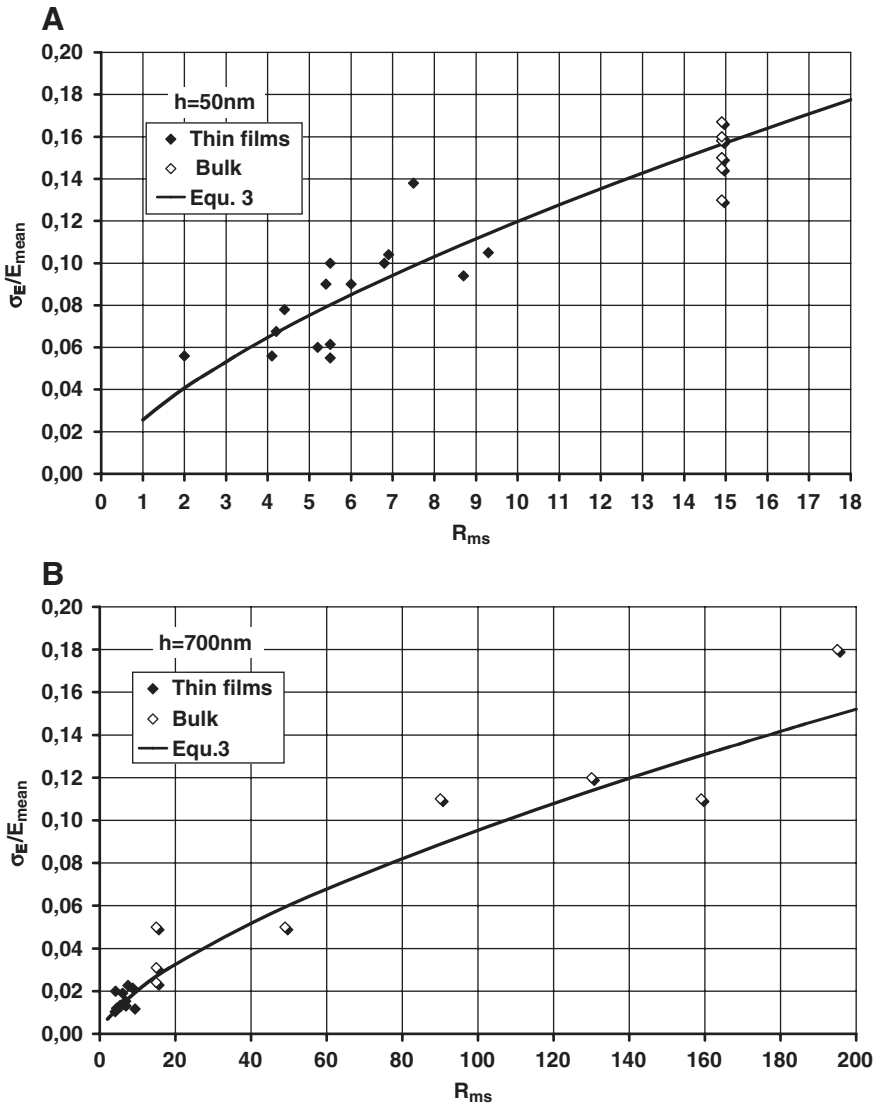

Fig. 4. (a) Example of variation of σ_E/E_{mean} versus R_{ms} for $h=50$ nm. Experimental results and representation of Eq. (3). (b) Example of variation of σ_E/E_{mean} versus R_{ms} for $h=700$ nm. Experimental results and representation of Eq. (3).

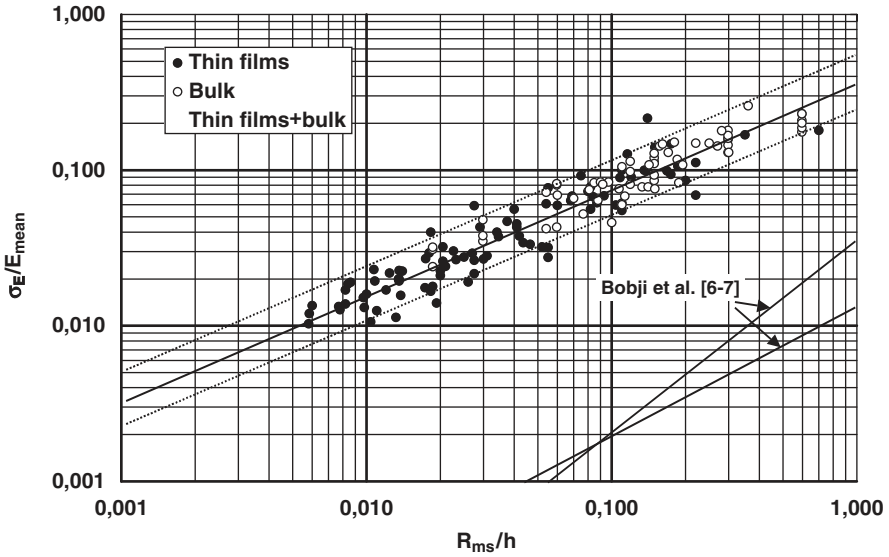

Fig. 5. Logarithmic variation of $\sigma_E/E_{mean}=f(R_{ms}/h)$ for all tested materials and for different indentation depths. Determination of Eq. (3).

materials nature, its roughness and the depth penetration. A linear regression leads to $n=0.66$ and $\beta=0.346$. It will be noted that all the points are around the representation of the Eq. (3) in a ratio ±1.5 (dotted lines on Fig. 5). However, in the case of thin films, the influence of the substrate is possibly not fully taken into consideration by the variation of E_{mean} versus h, and an additional dependence with the normalised indentation depth h/e_f could exist. In this aim, Fig. 6 represents $(\sigma_E/E_{mean})/(R_{ms}/h)^n=f(h/e_f)$ for different values of n close to 0.66 and we show that for $n=0.67$ this representation is independent of h/e_f while minimising the quadratic deviation with $\beta=0.35\pm0.15$. At last, Eq. (3) seems to be applied with the optimised parameters $n=0.67$ and $\beta=0.35\pm0.15$. The representations of this equation with those parameters are drawn on Fig. 4a, b for $h=50$ nm and $h=700$ nm. Thus, with a Berkovich indenter for an indentation depth ten times higher than roughness, a modulus can be hopefully measured with a margin of 7.5%. This value falls to 1.5% for a ratio h/R_{ms} equal to 100. For instance, electrolytic Ni for $J=2.5$ A dm^{-2} and $h\approx500$ nm gives approximately the same uncertainty (16%) than electrolytically polished Ni for $h\approx25$ nm (Fig. 3). This type of relation (Eq. (3)) is in agreement with the works of Bobji et al. [6,7], which report for σ_H/H_{mean} in the case of granite and sandstone, $n=0.83$ and $\beta=0.026$ for millimetric-length roughness with a random distribution and a spherical indenter [7], and $n=1.2$, $\beta=0.07$ for Cu with periodic pyramidal asperities of a millimetric-length indented with a spherical indenter [6]. Bobji et al. [7] showed that the ratio (σ_H/H_{mean}) is a slightly decreasing function of the roughness fractal D, which is connected to ξ exponent of the power law spectrum [23], that is to say:

$$D=\frac{5-\xi}{2} \tag{4}$$

Then exponent n decreases with D. The value of $n=0.83$ was calculated for a Brownian surface, that is to say $D=1.5$ ($\xi=2$)

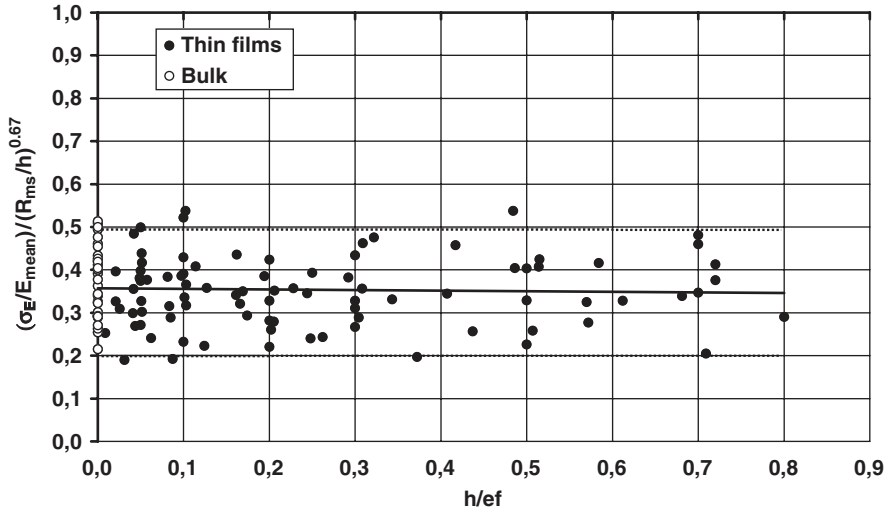

Fig. 6. Invariance of the ratio $(\sigma_E/E_{mean})/(R_{ms}/h)^{0.67}$ with the normalised indentation depth (h/e_f).

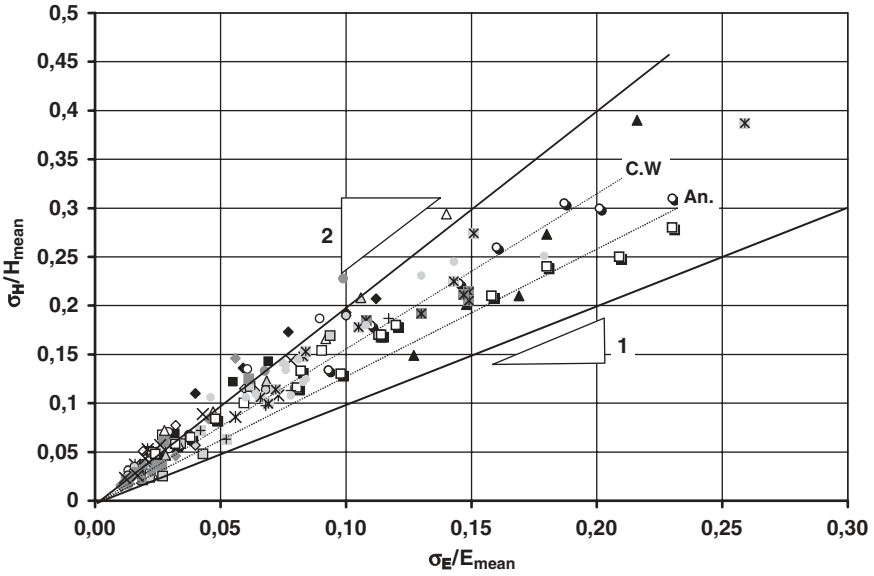

Fig. 7. Representation of $\sigma_H/H_{mean}=f(\sigma_E/E_{mean})$ for all tested materials.

[7]. Thus, if ξ decreases, the fractal D increases and then the exponent n decreases. This observation can possibly explain the value of $n=0.67$, which is lower than the value $n=0.83$ obtained numerically by Bobji et al. [7].

Concerning the ratio σ_H/H_{mean}, its dependence with σ_E/E_{mean} is reported on Fig. 7 for all used materials. It appears that this dependence is different from a material to another and between different films and bulk materials. Thus, a regression by a power law such as:

$$\frac{\sigma_H}{H_{mean}}=\delta\left(\frac{\sigma_E}{E_{mean}}\right)^{n_H} \tag{5}$$

gives respectively for the thin films and bulk materials $n_H=1.01$, $\delta=1.87$ and $n_H=0.92$, $\delta=1.25$. In both cases, n_H is very close to the unit and then a linear relation as the following can be proposed:

$$\frac{\sigma_H}{H_{mean}}=\delta\left(\frac{\sigma_E}{E_{mean}}\right)=\delta\cdot\beta\left(\frac{R_{ms}}{h}\right)^{n} \text{ with}$$
$$n=0.67 \text{ and } 1.2<\delta\leq 2 \tag{6}$$

For thin films, without the PMNT sample which presents disoriented crystallites at its surface, the point's dispersion from one specimen to another is very weak. It is not the same for the bulk samples.

In fact, considering in one hand the Eq. (2) and in the other hand that the loading and the unloading curves are, for a conical indenter, respectively given by [3,24]:

$$P_{load}=a\,h^2, P_{unload}=b(h-h_f)^q \text{ with } 1.2<q<1.5 \text{ thus}$$
$$S=\left(\frac{dP}{dh}\right)_{unload}=bq(h-h_f)^{q-1}dh \tag{7}$$

h_f being the remanent depth after the total unloading. The following relation can easily be obtained:

$$\frac{\Delta H}{H_{mean}}=2\frac{\Delta E}{E_{mean}}+2(2-q)\left(\frac{1-\frac{1}{2-q}\frac{h_f}{h}}{1-\frac{h_f}{h}}\right)\frac{\Delta h}{h} \tag{8}$$

ΔE and ΔH are the precision on the mean values of E and H. Moreover, for all the studied materials and for a large number of experiments, $25<\sum<45$, we experimentally found that

$$\frac{\sigma_E}{\Delta E}=\frac{\sigma_H}{\Delta H}=\alpha \text{ with } 1.21<\alpha<1.31 \tag{9}$$

This parameter is almost constant for large $\sum$ and it is interesting to notice, at last for the studied materials, that $\alpha=\frac{R_{ms}}{R_a}=1.29\pm0.08$, where R_a is the arithmetic mean of the roughness.

By combining Eqs. (8) and (9), the following expression is obtained:

$$\frac{\sigma_H}{H_{mean}}=2\frac{\sigma_E}{E_{mean}}+2(2-q)\alpha\left(\frac{1-\frac{1}{2-q}\frac{h_f}{h}}{1-\frac{h_f}{h}}\right)\frac{\Delta h}{h} \tag{10}$$

As $h_f\leq h$ and $\frac{h_f}{h}\geq 2-q$, at least for tested materials, the second term of Eq. (10) is negative, hence $\sigma_H/H_{mean}\leq 2\sigma_E/E_{mean}$, which is accordance with the previous statement $1<\delta\leq 2$. Moreover, α and q being different from one material to another, the term $\frac{h_f}{h}$ fluctuates, as well as the value of the parameter δ (Fig. 7). For a perfect elastic material, $h_f=0$, the loading and unloading curves are similar, so $q=2$, hence $\delta=2$. This case is close to those of the W, PZT and slightness to those of AlN and the different Cr configurations (Fig. 7). The value of

δ remains close to 2. The substrate that confines plasticity, preventing it to be developed, can also have an influence.

On the other hand, for a perfect plastic material $h/h_f=1$, no relation exists between E_{mean} and H_{mean} and Eq. (10) can no longer be applied. But, for an elastoplastic material, more the plastic component is high, more the ratio h/h_f increases and more the second term of Eq. (10) increases. This seems to be the case for Ni bulk samples. As an example on Fig. 7, the dependence of σ_H/H_{mean} according to σ_E/E_{mean} is drawn (doted lines) for various grains oriented <111>, <110>, <100> of bulk Ni and for annealed (An) and cold worked (C.W) states at 30% [16]. For these two states $\delta_{C.W}=1.55>\delta_{An}$. This observation is in accordance with Eq. (10). Indeed, according to Bolshakov and Pharr [24], the parameter q for a hardened material is higher than those for the annealed material and as $\left(\frac{h_f}{h}\right)_{An}\approx 0.94$ is only slightly higher than $\left(\frac{h_f}{h}\right)_{C.W}\approx 0.93$, this leads to $\delta_{C.W}>\delta_{An}$. Physically, this is explained by the hardening texture, which is strongly bimodal, made up of polygonation cells [25] and by taking into account the very low indentation depths, leads to a stronger dispersion on the value of σ_H than for recrystallized material [16,25].

On electroplated Ni sample having a great roughness ($R_{ms}=159$ nm for $J=2.5$ A dm^{-2}), Fig. 8 shows influence, on the modulus and the hardness, of a mechanical polishing using diamond paste, reducing roughness to $R_{ms}\approx 10\pm 5$ nm. For the same measured penetration depth the R_{ms}/h ratio decreases by a factor of about 16, which leads to a decrease of the standard deviation of a factor of around 6. Twenty-seven measurements by samples are considered and for various indentation depths the average values E_{mean} versus H_{mean}, as well as the associated standard deviations are reported. A slight increase of E_{mean} (5–6%) is observed as well as a decrease of H_{mean} (5–6%) with the polishing, but in an other hand, values of the standard deviation are completely different. In average, a ratio in the order of 6.6 on σ_E and σ_H is observed, which is in agreement with Eq. (3). For higher indentation depths, influence of polishing on the average value seems to disappear. The increase of E_{mean} can possibly be interpreted by the uncertainty on the determination of the contact. The area measured from the first contact on a rough surface is lower than a smooth one, hence the E_{mean} increasing (Eq. (2)). This uncertainty becomes insignificant for high indentation depth. It should be the same for the hardness (Eq. (2)), but on the other hand, the observed decreasing could reflect the influence of mechanical polishing on the inelastic properties on the material surface (ablation of Ni oxide, cyclic softening of material,...), the roughness decrease having no significant influence on hardness. Finally, for sufficiently large indentations numbers, roughness affects primarily the standard deviations σ_E and σ_H (Eqs. (3) and (10)) but slightly the average values E_{mean} and H_{mean}. The decrease of E_{mean} and H_{mean} with the indentation depth (E_{mean} ~230 GPa for $h=250$ nm and E_{mean} ~175 GPa for $h=1800$ nm) can be explained firstly by the columnar material nature, the colonies grains diameter being about 1 µm for a random orientation determined by EBSD, and secondly by a considerable porosity for this rather high current density. For small values of h, the measured values tend to be connected to a small crystallite number. For the higher indentation depth, the measure is more macroscopic and corresponds to an average of a high number of crystallites including the average effect of porosity. Moreover, it will be noted that for lowest current densities, porosity is less and the values of E_{mean} for $h=2000$ nm are higher [17,19]. In addition, the values need to be corrected from the pile-up effect [24], which is relatively significant (10% on E_{mean}) for this material [16].

The parameter β is found ($\beta=0.356$) with an order of magnitude higher than the values given by Bobji et al. [6,7] ($\beta=0.013$ and 0.035 for $\delta=2$ in the Eq. (6)) for a spherical indenter and for millimetric-length roughness (full lines on Fig. 5). This parameter β depends on the ratio between the indenter radius R_i and the indented asperity R_a for the very small indentation depths [8]. For higher indentation depths (h/

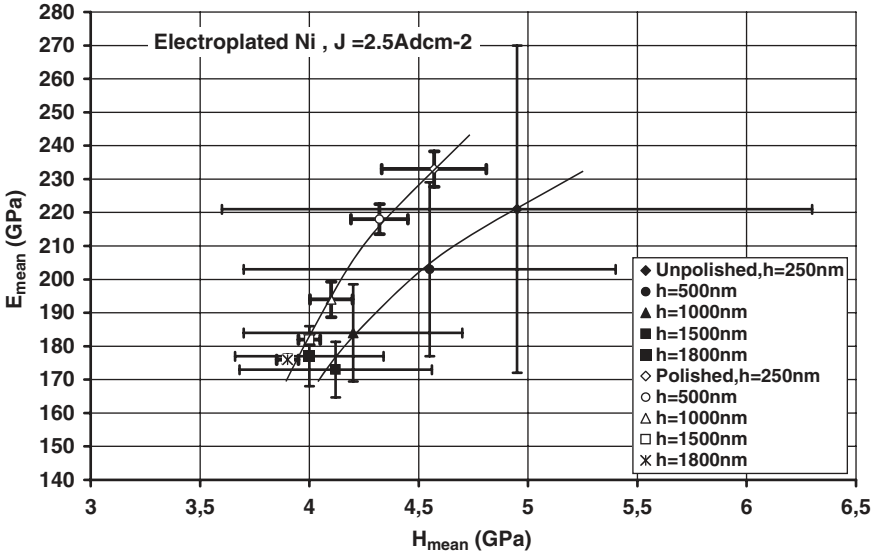

Fig. 8. Influence, for electroplated Ni at $J=2.5$ A dcm^{-2}, of the mechanical polishing on the values of E_{mean}, H_{mean}, σ_E and σ_H and for different indentation depths.

$R_{ms} \geq 10$), and for a given geometry, at first approximation the standard deviation is suggested depending on the relationship between the contact perimeter and the contact surface between the indenter and the materials. In the case of spherical cap, this ratio varies like $1/\sqrt{R_i h}$, here this ratio is a decreasing function of R_i for a fixed h. This observation could explain the small value of β for a spherical indenter having a larger radius of curvature than for a Berkovich indenter.

As a conclusion and generally, Eqs. (3) and (6) could be rewritten in the following form:

$$\frac{\sigma_E}{E_{mean}} = \beta\left(\frac{R_{ms}}{h}\right)^n \text{ with } n = f(D) \text{ and } \beta = g(\theta, R_{i,\ldots}) \quad (11)$$

$$\frac{\sigma_H}{H_{mean}} = \delta\left(\frac{\sigma_E}{E_{mean}}\right) \text{ with } \delta \leq 2$$

depending on the material's plasticity,

functions f and g remaining to be specified. It is pointed out that D is the roughness fractal, θ the indenter angle and R_i his radius of curvature.

4. Conclusion

Using the compilation of the experimental results of the Berkovich nanoindentation tests made on various materials (thin films and bulk) presenting different roughness, the influence of the roughness parameter R_{ms} on the standard deviations σ_E and σ_H of the average values of Young' modulus and hardness E_{mean}, H_{mean} has been quantified. A power law is reported between σ_E/E_{mean}, σ_H/H_{mean} and (R_{ms}/h), h being the indentation depth. This law is in accordance with the works of Bobji et al. [6,7]. Moreover, the relationship between σ_E/E_{mean} and σ_H/H_{mean} is clarified. These two relations are illustrated and discussed starting from two different situations, which are firstly the influence of the cold working and secondly the mechanical polishing on the average values and the standard deviations.

References

[1] J.L. Loubet, J.M. Georges, O. Marchesini, J. Tribol. 106 (1984) 83.
[2] M.F. Doerner, W.D. Nix, J. Mater. Res. 1 (1986) 601.
[3] W.C. Oliver, G.M. Pharr, J. Mater. Res. 7 (1992) 1564.
[4] G.M. Pharr, Mater. Sci. Eng., A 253 (1998) 151.
[5] J. Mencik, M.V. Swain, J. Mater. Res. 10 (1995) 1491.
[6] M.S. Bobji, S.K. Biswas, Tribol. Lett. 7 (1999) 51.
[7] M.S. Bobji, K. Shivakumar, H. Alehossein, V. Venkateshwarlu, S.K. Biswas, Int. J. Rock Mech. Min. Sci. 36 (1999) 399.
[8] M.S. Bobji, S.K. Biswas, J. Mater. Res. 15 (11) (1998) 3227.
[9] G. Velu, D. Remiens, B. Thierry, J. Eur. Ceram. Soc. 17 (1997) 1749.
[10] P. Delobelle, E. Fribourg-Blanc, O. Guillon, E. Cattan, D. Remiens, Integr. Ferroelectr. 69 (2005) 213.
[11] K. Tsubauchi, K. Sugai, N. Nikoshiba, IEEE Utrasonics Symposium, 1981, p. 375.
[12] A. Bosseboeuf, M. Dupeux, M. Boutry, T. Bouriouna, D. Bouchier, D. Débarre, Microsc., Microanal., Microstruct. 8 (1997) 261.
[13] M. Qasmi, P. Delobelle, F. Richard, A. Bosseboeuf, Surf. Coat. Technol. 200 (2006) (10 pp).
[14] J. Lintymer, N. Martin, J.M. Chappé, P. Delobelle, J. Takadoum, Surf. Coat. Technol. 180–181 (2004) 26.
[15] J. Lintymer, N. Martin, J.M. Chappé, P. Delobelle, J. Takadoum, Surf Coat. Technol. 200/1–4 (2004) 269.
[16] P. Delobelle, H. Hadou, X. Feaugas, Matériaux 2002, CM1101.PDF, 21–25 Oct., 2002, Tours, France.
[17] S. Basrour, P. Delobelle, Mater. Res. Soc. Symp. Proc. 657 (2001) EE4.1.1.
[18] S.W. Banovic, K. Barmak, A.R. Marder, J. Mater. Sci. 33 (1998) 639.
[19] T. Fritz, M. Griepentrog, W. Mokwa, U. Schnakenberg, Electr. Acta 48 (2003) 3029.
[20] R.B. King, Int. J. Solid Struct. 23 (12) (1987) 1657.
[21] A.K. Bhattacharya, W.D. Nix, Int. J. Solid Struct. 24 (12) (1988) 1287.
[22] R. Saha, W.D. Nix, Acta Mater. 50 (2002) 23.
[23] K. Ventatesh, M.S. Bobji, S.K. Biswas, J. Mater. Res. 14 (2) (1999) 319.
[24] A. Bolshakov, G.M. Pharr, J. Mater. Res. 13 (4) (1998) 1049.
[25] H. Haddou, C. Gaudin, X. Feaugas, 4th Euromech Mecamat, PMMP, Metz 26–29 June, 2002.